

## Rheological texture in a journal bearing with magnetorheological fluids

Lampaert, Stefan G.E.; Quinci, Federico; van Ostayen, Ron A.J.

**DOI**

[10.1016/j.jmmm.2019.166218](https://doi.org/10.1016/j.jmmm.2019.166218)

**Publication date**

2020

**Document Version**

Final published version

**Published in**

Journal of Magnetism and Magnetic Materials

**Citation (APA)**

Lampaert, S. G. E., Quinci, F., & van Ostayen, R. A. J. (2020). Rheological texture in a journal bearing with magnetorheological fluids. *Journal of Magnetism and Magnetic Materials*, 499, Article 166218. <https://doi.org/10.1016/j.jmmm.2019.166218>

**Important note**

To cite this publication, please use the final published version (if applicable). Please check the document version above.

**Copyright**

Other than for strictly personal use, it is not permitted to download, forward or distribute the text or part of it, without the consent of the author(s) and/or copyright holder(s), unless the work is under an open content license such as Creative Commons.

**Takedown policy**

Please contact us and provide details if you believe this document breaches copyrights. We will remove access to the work immediately and investigate your claim.



ELSEVIER

Contents lists available at ScienceDirect

## Journal of Magnetism and Magnetic Materials

journal homepage: [www.elsevier.com/locate/jmmm](http://www.elsevier.com/locate/jmmm)

## Research articles

## Rheological texture in a journal bearing with magnetorheological fluids

Stefan G.E. Lampaert<sup>a,\*</sup>, Federico Quinci<sup>b</sup>, Ron A.J. van Ostayen<sup>a</sup><sup>a</sup> Delft University of Technology, Mekelweg 2, 2628 CD Delft, the Netherlands<sup>b</sup> Bifrost Research and Development B.V., Molenvliet 34, 3961 MV Wijk bij Duurstede, the Netherlands

## ARTICLE INFO

## Keywords:

Magnetic fluid  
Bingham plastic  
Numerical modelling  
Magnetism  
Rheology  
Fluid mechanics

## ABSTRACT

This paper discusses a new type of hybrid journal bearing in which a magnetorheological fluid is used in combination with local magnetic fields, such that the hydrodynamic and hydrostatic working regimes are not compromised. This demonstrates the potential of using the concept of rheological texture in bearings. The performance of this new type of bearing is assessed via Finite Element Modelling (FEM) in which the behaviour of the fluid film is described by the ideal Bingham plastic fluid model. Both the yield stress and the viscosity increase as a function of the magnetic field.

## 1. Introduction

Bearing systems have been under a huge development for the last half century at least [1,2]. The presentation of the so-called “Jost Report” in 1966 gave recognition to the huge impact that bearings hold in our society [3]. For example, Holmberg & Erdemir estimated that about 23% (119EJ) of the world’s total energy is lost in tribological contacts [4].

Although decades of research and development have passed after the “Jost Report”, little conceptual development in bearing design has occurred.

Some effort has been made in the field of tribotronics to seek for new bearing concepts, where the potential is investigated of adding control systems to the bearing [5,6]. Likewise, new bearing concepts based on magnetism that use either ferrofluids [7–10] or magnetorheological fluids [11–20] have been explored. In a similar fashion, electrorheological fluids are investigated for a possible use in bearing systems [21–24]. The current work focuses on the use of magnetorheological fluid in journal bearings.

Hydrodynamic journal bearings are used pervasively in all types of machine design due to their cost-effective, superior friction and wear properties [25]. The bearing system consists of a cylindrical shaft inside a cylindrical bush, where the gap between the two is filled with lubricant. This geometry allows the shaft and housing to be able to freely rotate with respect to each other (Fig. 1a). The rotation, together with the converging wedge caused by eccentricity, creates a high-pressure region counteracting the eccentric position. The shaft is floating into this lubricating layer that guarantees a low wear and friction. The main drawback of this bearing configuration is that at low speeds the load

carrying capacity of the lubricating film might be incapable to sustain the load, thus leading the two surfaces into physical contact. This causes excessive friction and wear that may lead to system failure eventually.

One efficient way to overcome this drawback is to use a hydrostatic journal bearing instead (Fig. 1b). This concept uses a high-pressure lubricant supply which is supplied into large surface area recesses to make sure that the shaft floats in the lubricating film during high loads for both low and high speeds. However, the drawback of this design is that the high-pressure hydraulic supply is sensitive to failure, which fact moves the problem to another component in the system. The failure of the pump causes excessive wear in the bearing as it operates very poorly in the hydrodynamic regime due to the surface texture.

The ideal bearing combines the low friction and wear at high speeds with the high load capacity at low speeds. The type of bearing that meets these requirements is the hybrid journal bearing (Fig. 1c). In detail, this concept combines the smooth bearing surface of a hydrodynamic bearing with the high pressure supply of a hydrostatic bearing. In this way, it achieves sufficiently low wear and sufficiently high load capacity for the complete range of speeds and loading conditions. When the pump fails, the hybrid journal bearing reverts to a hydrodynamic journal bearing. The drawback of this concept is that the hydrostatic load capacity is limited due to the absence of surface recesses.

The three concepts in Fig. 1a, b and c share the fact that a modification in the geometry of the bearing surface causes changes in the bearing performance. Specifically, a physical change in the surface texture leads to a change in the film height, which in turn modifies locally the lubricant flow resistance. Controlling this local resistance is key to improve the performance of the bearing [26,27].

\* Corresponding author.

E-mail address: [S.G.E.Lampaert@tudelft.nl](mailto:S.G.E.Lampaert@tudelft.nl) (S.G.E. Lampaert).<https://doi.org/10.1016/j.jmmm.2019.166218>

Received 29 July 2019; Received in revised form 13 November 2019; Accepted 26 November 2019

Available online 29 November 2019

0304-8853/ © 2019 The Authors. Published by Elsevier B.V. This is an open access article under the CC BY license

<http://creativecommons.org/licenses/by/4.0/>.

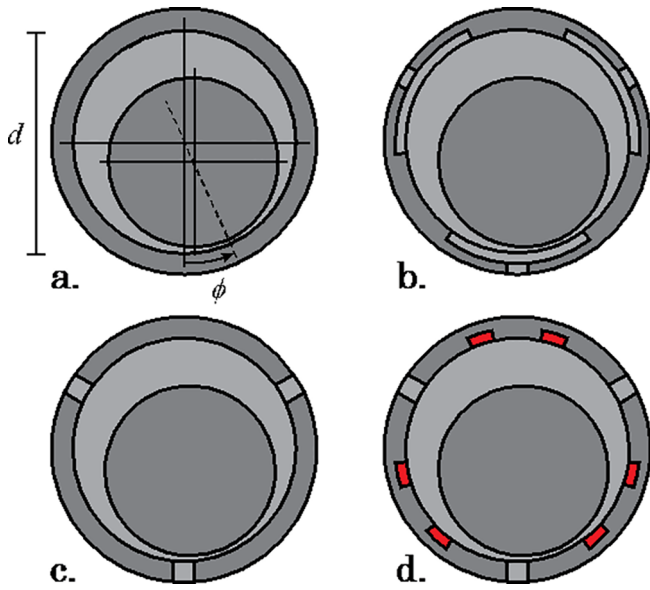


Fig. 1. a: Hydrodynamic journal bearing, b: hydrostatic journal bearing, c: hybrid journal bearing, d: hybrid journal bearing with rheological texture.

A possible approach to manipulate the flow resistance, other than changing the geometry, is to locally vary the rheological properties of the lubricant. This fluid manipulation is addressed as rheological texture and it can be carried out by using a magnetorheological fluid whose rheological properties change in response to a local variation of the magnetic field [28,29]. Based on the rheological texture, multiple new bearing configurations can be conceived that all have unique performance [30].

This paper demonstrates the potential of using the concept of rheological texture in journal bearings. The work discusses a new type of hybrid journal bearing in which a magnetorheological fluid is used in combination with local magnetic fields so as the hydrodynamic and hydrostatic working regimes are not compromised (Fig. 1d). In addition, the work discusses a herringbone bearing that uses the rheological texture in a v-shaped pattern. The performance is assessed in a FEM platform (COMSOL Multiphysics® 5.4) in which the ideal Bingham plastic fluid model is used to predict the behaviour of the fluid film. Both the yield stress and the viscosity increase as a function of the magnetic field.

## 2. Method

This study makes use of different journal bearing configurations as showcases to present the effect of including rheological textures in a bearing device. This work considers hydrostatic journal bearings with rheological texture, hybrid journal bearings with rheological texture and hydrodynamic journal bearings with the rheological texture in a herringbone-like v shape. Figs. 1–3 show both conventional hydrodynamic as well as hydrostatic journal bearing configurations considered in this investigation. In addition, a hydrodynamic bearing with a herringbone rheological textures is shown in Fig. 4.

For a fair comparison, the different configurations are tested against a conventional journal bearing. The lubricant in the bearing is modelled as a Bingham plastic and its flow is modelled using the Reynolds equations resulting from the standard thin film fluid flow assumptions. Tables 1 and 2 specify the different parameters used by the different bearing configurations.

The fluid film height  $h$  for all bearing configurations is described in relation (Eq. (1)). The eccentricity value  $e$  is the relative amount that the shaft is eccentric with respect to the housing. Its value is zero when the shaft is exactly in the middle and one when the shaft is touching the

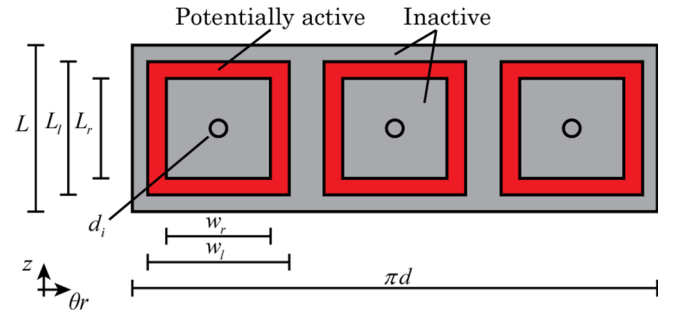


Fig. 2. Unfolded hybrid journal bearing (Fig. 1d) with rheological texture and three pads.

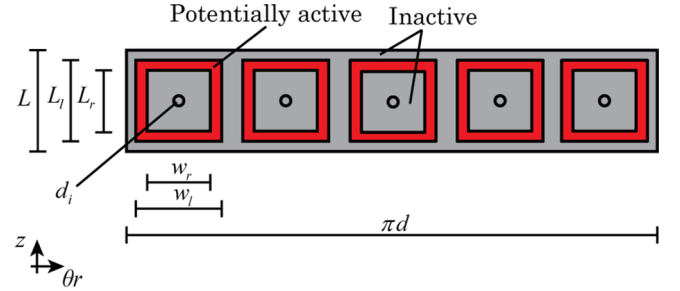


Fig. 3. Unfolded hybrid journal bearing (Fig. 1d) with rheological texture and five pads.

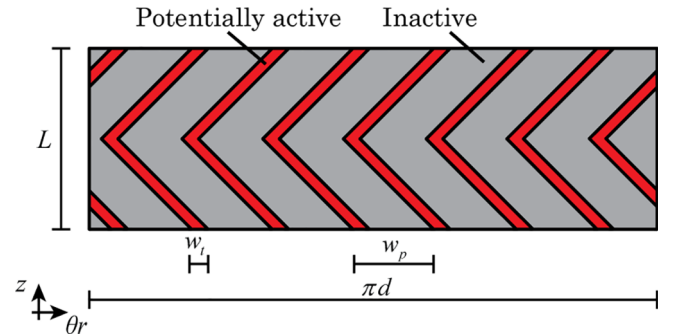


Fig. 4. Unfolded version of the hydrodynamic journal bearing with rheological textures in the shape of a herringbone.

Table 1  
General model parameters used.

Variable	Symbol	Value
Bearing diameter	$d$	0.2[m]
Viscosity	$\eta_g$	0.05[Pa·s]
Clearance	$c$	$d/500$
Eccentricity	$e$	0.7
Speed	$v$	100[rpm]

Table 2  
Model parameters for the bearing configurations presented in Figs. 2 and 3.

Inlet diameter	$d_i$	$L\Delta/n$
Land width factor	$\Delta$	0.8
Land length	$L_l$	$L(1 - \Delta)$
Recess length	$L_r$	$L(1 - 2\Delta)$
Land width	$w_l$	$\pi d/n(1 - \Delta)$
Recess width	$w_r$	$\pi d/n(1 - 2\Delta)$
Restrictor value	$R$	$10^4 \text{m}^4/\text{N}^2 \text{s}$
Location of minimum film height	$\phi$	$-\pi/12$

**Table 3**  
Model parameters for the bearing configurations presented in Figs. 2 and 3.

	Non-Activated	Activated
Hydrodynamic	$p_s = 0Pa\eta_a = \eta_g\tau_0 = 0$ (Fig. 5a)	$p_s = 0Pa\eta_a = 20\eta_g\tau_0 = 500Pa$ (Fig. 5c)
Hybrid	$p_s = 10^6Pa\eta_a = \eta_g\tau_0 = 0$ (Fig. 5b)	$p_s = 10^6Pa\eta_a = 20\eta_g\tau_0 = 500Pa$ (Fig. 5d)

housing. The variable  $\theta$  presents the angular coordinate in the bearing and the variable  $\phi$  presents the angular offset where the film height has its minimum.

$$h = c(1 - \text{ecos}(\theta + \phi)) \quad (1)$$

The numerical model solves for the pressure in the lubricating film that leads to a load capacity  $F_r$  by taking the vector sum of the load capacity in x-direction  $F_x$  and y-direction  $F_y$  in relations (Eqs. (2)–(4)). The resulting load capacity is one of the output variables of the computation.

$$F_x = \iint_S p \sin(\theta) dA \quad (2)$$

$$F_y = \iint_S p \cos(\theta) dA \quad (3)$$

$$F_r = \sqrt{F_x^2 + F_y^2} \quad (4)$$

The friction force of the bearing is expressed by relation (Eq. (5)). The parameter  $\tau_x$  is the amount of stress that is locally present to achieve the desired relative motion of the two surfaces. The friction coefficient  $f$  in (Eq. (6)) is calculated as the ratio between the load capacity  $F_r$  in (Eq. (4)) and the friction force of the bearing  $F_f$  in (Eq. (5)). To include the effects of cavitation, all negatives pressures are assumed to be zero.

$$F_f = \iint_S -\tau_{\theta r} - \frac{h}{2} r \frac{\partial p}{\partial \theta} dA \quad (5)$$

$$f = \frac{F_r}{F_f} \quad (6)$$

### 2.1. Rheological model

The Bingham plastic fluid model presented in (Eq. (7)) accommodates for a proper representation of the rheological behaviour of the magnetorheological fluid by presenting the stress in the material  $\vec{\tau}$  as a function of the shear rate  $\dot{\gamma}$ . The use of a magnetic field affects both the yield stress  $\tau_0(H)$  as well as the viscosity of the fluid  $\eta(H)$ . The values are based on typical values from literature [29].

$$|\vec{\tau}| = \tau_0(H) + \eta(H)|\dot{\gamma}| \quad (7)$$

### 2.2. Thin film model

The flow in-between the two bearing surfaces is described by a mathematical model developed by the authors and published in [31]. The model derives a modified Reynolds equation that uses the exact Bingham plastic material model to simulate the thin film flow. The novelty is that in this way, there is no need for either a regularization technique [32] or an approximated thin film theory [33–35]. Since the method is not an approximation, the solution is more accurate and the simulation “running time” is considerably shortened due to the reduced degrees of freedom of the simulation.

### 2.3. Hybrid bearing

Figs. 2 and 3 illustrate an unfolded version of different bearing configurations to demonstrate the behaviour of a hybrid bearing with

rheological texture. The figures show three and five squares respectively over which the fluid can be activated to create a rheological texture. Note that the viscosity is increased and the limiting yield stress is active at these locations.

In practice, this effect can be associated to the application of a magnetic field that locally increases the effective viscosity of the magnetorheological fluid.

The fluid behaves as a Newtonian fluid everywhere else, that is, the yield stress of the fluid is zero since there is no magnetic field. The circles located in the middle of the bearing (Figs. 1 and 3) serve as high-pressure lubricant supply to make a hydrostatic bearing. An orifice restrictor controls the amount of lubricant supplied to the bearing. The relation presented in (Eq. (8)) represents the behaviour of the restrictor in this study. The variable  $R$  presents the restrictor value and the parameter  $p_r$  presents the recess pressure.

$$Q = R\sqrt{p_s - p_r} \quad (8)$$

The behaviour of a conventional hydrodynamic bearing is obtained when both rheological texture and supply pressure are switched off.

A conventional hybrid bearing is attained by only applying the feeding pressure without local activation of the fluid. The condition in which the fluid is locally activated and the supply pressure is not applied generates a hydrodynamic bearing with rheological texture. On the other hand, by locally activating the fluid and applying the supply pressure generates a hybrid bearing configuration with rheological texture.

Tables 1 to 3 list the values of the different parameters used to generate the results presented in this paper. These are typical values of bearings in this size category. The fluid properties are typical for magnetorheological fluids available on the market (silicon oil with ~70w% iron particles).

### 2.4. Herringbone

Fig. 4 presents the unfolded geometry of the herringbone journal bearing configuration which is presented here to demonstrate the effect of applying rheological texture for hydrodynamic lubrication exclusively. The figure shows seven v-shaped areas where the lubricant can be activated to create a rheological texture. Table 4 shows the parameters specific to this simulation, while Table 1 presents all other relevant parameters.

## 3. Results & discussion

### 3.1. Hybrid bearing

Fig. 5a to d illustrate the pressure distributions for the four different

**Table 4**  
Model parameters for the herringbone bearing presented in Fig. 4.

Variable	Symbol	Value
Land width factor	$\Delta$	0.9
Bearing length	$L$	$d$
Location of minimum film height	$\phi$	0
Texture width	$w_t$	$L\Delta$
Texture pitch	$w_p$	$\pi d/7$

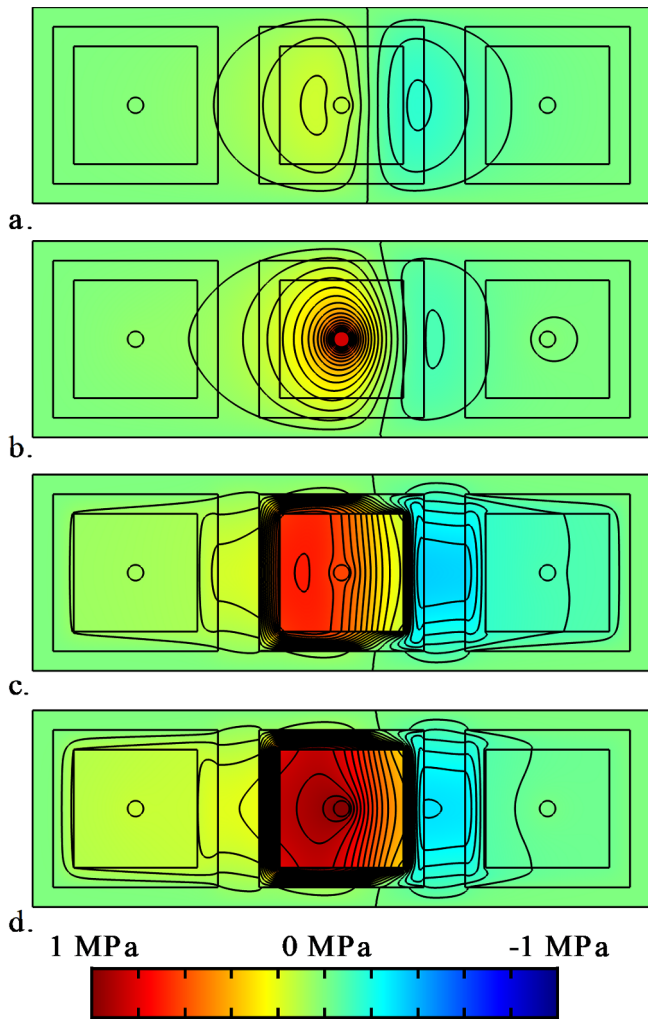


**Fig. 5.** a. Pressure distribution of a. conventional hydrodynamic bearing with non-activated regions b. conventional hybrid bearing with non-activated regions c. hydrodynamic bearing with activated regions d. hybrid bearing with Rheological textures.

configurations considered in this work. Note that these pressure distributions are presented on the unfolded geometries of the journal bearing configurations presented in Fig. 1. Table 3 presents the corresponding parameter values for these four different situations. Note that the results use a zero pressure reference, which means that in practice cavitation will occur when the pressure is negative. Since the focus of this work is on the resulting pressure distribution due to rheological textures, only a basic cavitation model is included that assumes all negative pressures to be equal to zero.

Fig. 5a displays the pressure distribution of a conventional journal bearing. There is a high-pressure region in the converging wedge and a low-pressure region in the diverging wedge. The central pressure supply shows a slight change in the pressure distribution due to a local change in distance between the bearing faces.

Fig. 5b shows the pressure distribution of a conventional hybrid journal bearing. A high-pressure region exists near the high-pressure supply at the converging part of the bearing. A low-pressure field exists at the diverging wedge of the bearing. Note that the pressure supply increases the both high-pressure and low-pressure fields more than is the case for the conventional hydrodynamic bearing. This causes less cavitation in the converging wedge.

Fig. 5c shows the pressure distribution of a hydrodynamic bearing with rheological texture. The figure shows a high-pressure field at the converging part of the bearing and a low-pressure field at the diverging

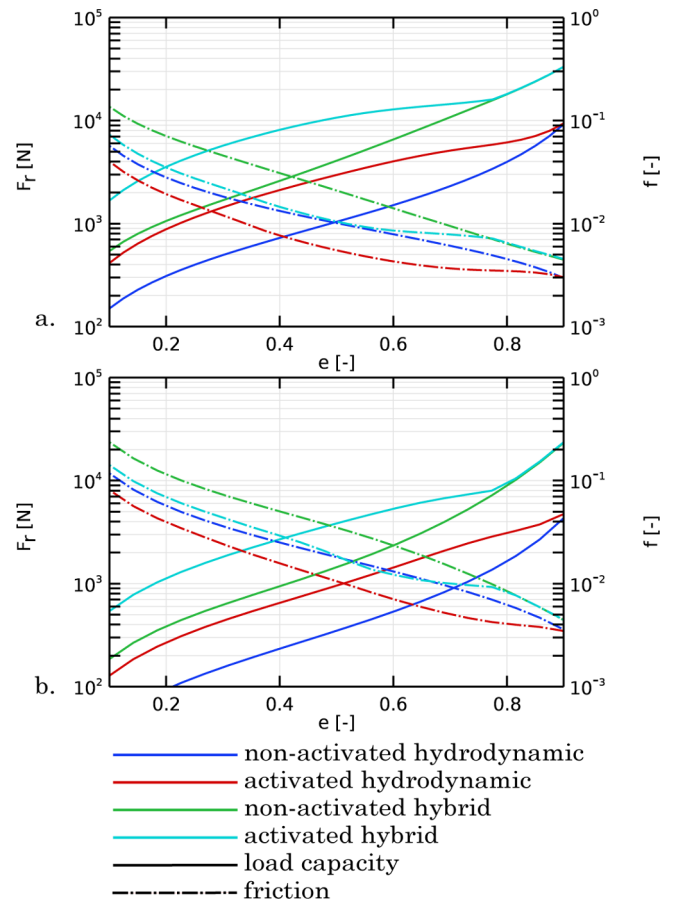


**Fig. 6.** a. Bearing load capacity and friction coefficient as a function of the eccentricity for the 3-pad bearing. b. Bearing load capacity and friction coefficient as a function of the eccentricity for the 5-pad bearing.

part of the bearing. By comparing this pressure distribution with the one in Fig. 5a for the conventional hydrodynamic bearing, it is clear that the rheological texture definitely affects the pressure distribution. The figure indicates first that the magnitude of the pressure is greater than that shown by the conventional hydrodynamic bearing, and secondly that the rheological texture causes a high pressure region within the activated square annulus. In addition, the area with cavitation presents now a low-pressure field located in-between the two square annuli.

Fig. 5d shows again a high-pressure field within the activated square annulus at the converging wedge. The annulus creates an even higher-pressure field due to the high-pressure supply. This behaviour is very similar to the conventional hydrostatic bearing where a high-pressure field is present in the recess of the bearing. The area within the square annulus acts as a recess area and the square annulus itself acts as a pad area of a hydrostatic bearing. Again, the area in-between the two right square annuli has a low-pressure field.

Fig. 6a and b show the load capacity and friction coefficient as a function of the eccentricity for both 3-pad and 5-pad bearing respectively. The dark blue line and the green line stand for the conventional hydrodynamic journal bearing and the hybrid journal bearing respectively. The conventional hybrid journal bearing has a higher load capacity and lower friction coefficient at low eccentricity ratios but this difference becomes smaller for large eccentricity ratios. This effect is explained by the fact that the hydrostatic effect has only a small influence at low eccentricity due to the limited supply pressure. These results are in good accordance with other studies in literature [25,31,32,36].

The green line and the cyan line represent the hydrodynamic

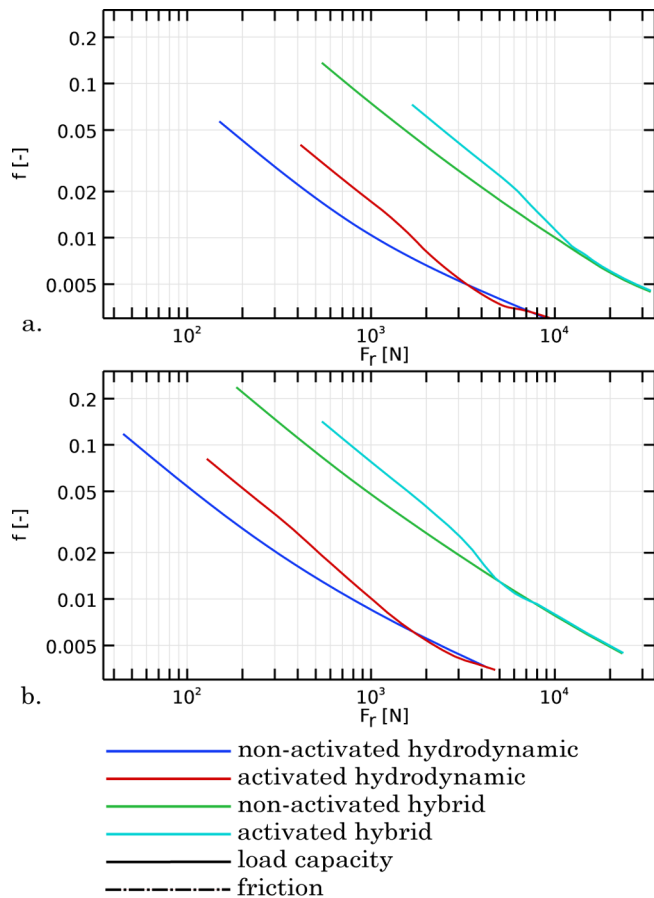


Fig. 7. Friction coefficient as a function of the load capacity for the same data as Fig. 6. Figure a presents the 3-pad bearing and figure b presents the 5-pad bearing.

journal bearing and hybrid journal bearing respectively both with rheological texture. Results show with clarity that the load capacity of the configurations with rheological texture significantly increases compared to the non-activated configurations at all eccentricity values. Also interesting to note here is that the stiffness remains roughly the same after applying the rheological texture. These results also make evident the fact that the friction coefficient generally increases when rheological texture is applied for a certain eccentricity ratio.

The results for the 3-pad bearing and 5-pad bearing are similar in shape. The load capacity and friction coefficient are higher for the 3-pad configuration than for the 5-pad configuration for a given eccentricity value. This means that making the bearing shorter does not necessarily produce a positive effect for the friction coefficient in this particular situation, although the negative effect is almost negligible.

Fig. 7a and b show the friction coefficient as a function of the load capacity by using the same set of data in Fig. 6. The figure illustrates whether a certain bearing configuration has a lower friction coefficient for a certain loading condition. Once more, it is evident that the friction coefficient generally increases when rheological texture is applied. Hybrid bearing configurations have a higher friction coefficient at low loading conditions but a slightly lower friction coefficient at high loading conditions compared to purely hydrostatic bearing configurations. The 3-pad and 5-pad bearing configuration present a similar trend.

Fig. 8a and b show the load capacity and friction coefficient as a function of the speed for the 3-pad and 5-pad configuration respectively. The green and dark blue line stand for the hydrodynamic journal bearing configurations with and without rheological texture respectively. The results demonstrate that the rheological texture causes the

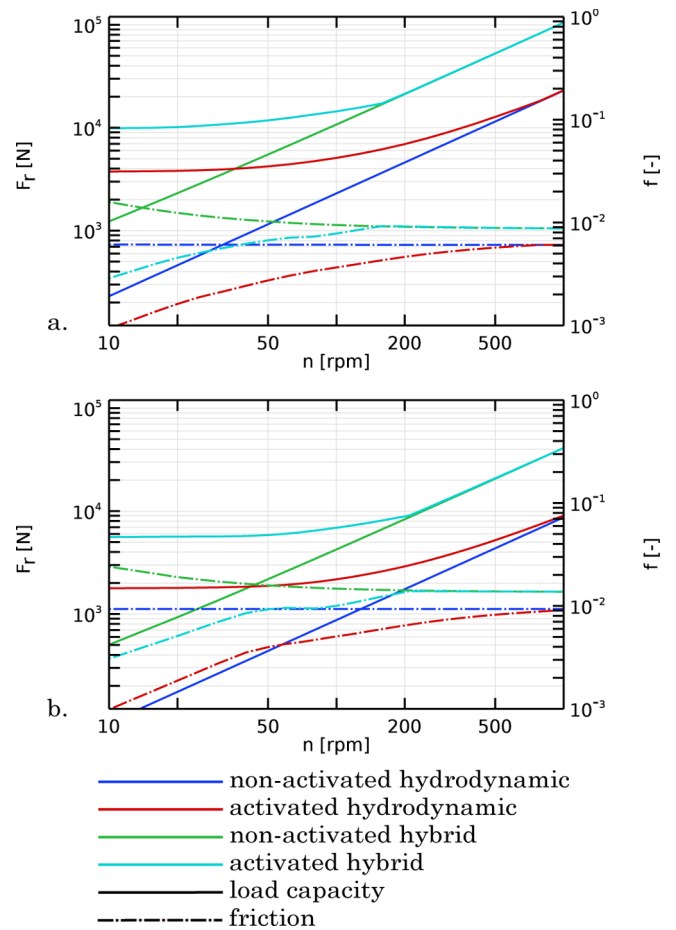


Fig. 8. Bearing load capacity and friction coefficient as a function of the speed of a. 3-pad bearing configuration and b. the 5-pad bearing configuration.

load capacity and friction coefficient to shift towards higher values. Note that the conventional hydrodynamic journal bearing exhibits a constant friction coefficient with increasing speed, while the corresponding hydrodynamic journal bearing with rheological texture shows an increase in friction coefficient at lower speeds instead. This outcome can be attributed to the behaviour of the lubricant, which is modelled as a Bingham material at the location of the rheological textures. The yield stress of the lubricant has a large effect at low speeds but only a small effect at high speeds in this specific circumstance.

The light blue and red line symbolize the hybrid journal bearing configurations with and without rheological texture respectively. Again, these results demonstrate that the rheological texture causes the load capacity as well as the friction coefficient to shift towards higher values. Hybrid bearing configurations work predominantly in hydrostatic regime at low speeds and predominantly in hydrodynamic regime at high speed, as expected.

In general, results reveal that load capacity increases significantly by applying the rheological texture for both the hydrostatic and the hydrodynamic regimes. This indicates that the method increases the specific load capacity (load per area) of the bearing. However, the price to pay for the local activation of the lubricant seems to be an increase in friction coefficient (load capacity per friction).

The hybrid journal bearing with rheological texture shows a very similar behaviour to that of a conventional hydrostatic bearing with physical texture. When the high pressure lubricant supply in this type of bearing is turned off, the presence of the physical texture causes an insufficient build-up of hydrodynamic pressure in the lubricant film, thus easily leading the two bearing surfaces into contact for already a minimal load, with unwanted side effects like wear.

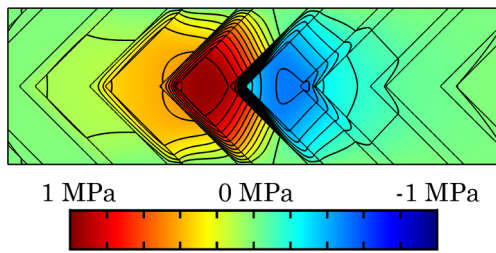


Fig. 9. Pressure profile of the herringbone bearing.

On the contrary, this condition would not cause severe damage in the hybrid bearing with rheological texture since it will just continue to operate in the hydrodynamic regime.

In the standard design of a hydrostatic bearing using geometric texture the hydrodynamic pressure build-up is compromised. Surface texture needed for a proper hydrostatic operation reduce the hydrodynamic operation. The use of rheological texture avoids this downside.

### 3.2. Herringbone

Fig. 9 shows the pressure distribution of the hydrodynamic bearing configuration with a rheological texture in the shape of a herringbone. As in Figs. 5,9 shows that the application of the rheological texture significantly changes the pressure distribution in the journal bearing. The texture causes the magnitude in the high-pressure field to increase and in the low-pressure side to decrease.

Fig. 10 shows both load and friction of the herringbone bearing as a function of the rotational speed. The dark blue line again represents the standard untextured hydrodynamic bearing identical to the hydrodynamic bearing configuration in Fig. 8. The green line represents the situation in which the rheological texture only has an increase in viscosity while the red line represents the situation where the rheological texture has an increase in both viscosity and yield stress. The inclusion of the yield stress causes higher load capacity as well as higher friction coefficient at low speeds but not much of a difference in case of high speeds. From this, it is assumed that the effect of the yield stress is in general negligible at higher speeds.

The cyan coloured lines represent the load capacity and friction coefficient of a purely hydrodynamic bearing with an increased viscosity compared to the situation of the standard hydrodynamic bearing. In this case, the viscosity is equal to the average viscosity of the

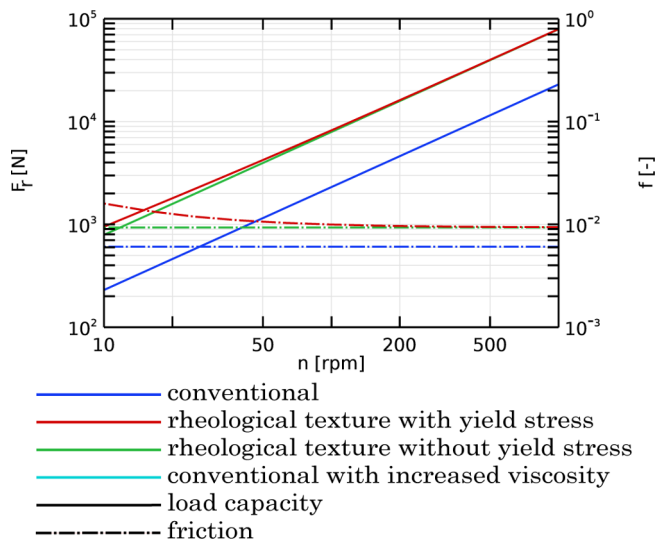


Fig. 10. Load and friction of the herringbone bearing as a function of the rotational speed. Note that the dark and light blue dash-dot line coincide.

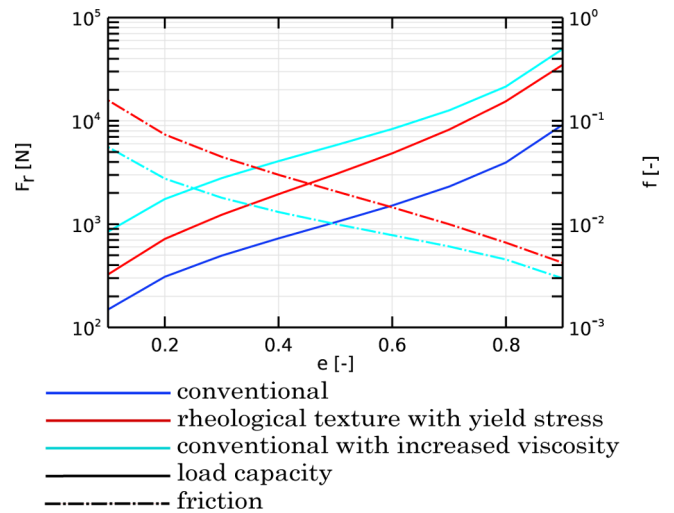


Fig. 11. Load and friction of the herringbone bearing as a function of eccentricity.

hydrodynamic bearing with no yield stress applied (green line). By averaging the viscosity, the resulting friction force of the two concepts is equal. This leads to a fair comparison between using rheological texture and increasing the viscosity in a uniform way. The results in Fig. 10 demonstrate that the rheological texture does not result in a lower friction coefficient, meaning that it does not create more load capacity per unit friction of the bearing. In other words, the use of rheological texture increases the load capacity of the bearing but not as efficiently as changing the viscosity uniformly. Note that this conclusion is only valid for this specific herringbone bearing configuration.

Fig. 11 presents the load and friction of the herringbone bearing as a function of the eccentricity. The dark blue line indicates the situation of the conventional hydrodynamic bearing, while the red line indicates the case of a hydrodynamic bearing with rheological texture (including yield stress). The cyan line represents the conventional hydrodynamic bearing configuration with a uniformly increased viscosity such that the average viscosity is equal to the average viscosity of the bearing configuration with rheological texture. The figure supports the statement that the load capacity and friction coefficient of the configuration with rheological texture scales in a similar way as the configuration without rheological texture. In addition, the assertion stating that the application of the rheological texture increases the load capacity of the bearing but not as efficiently as changing the viscosity uniformly still holds.

Fig. 12 shows the load and friction of the herringbone bearing as a function of the viscosity at the location of the rheological texture for a

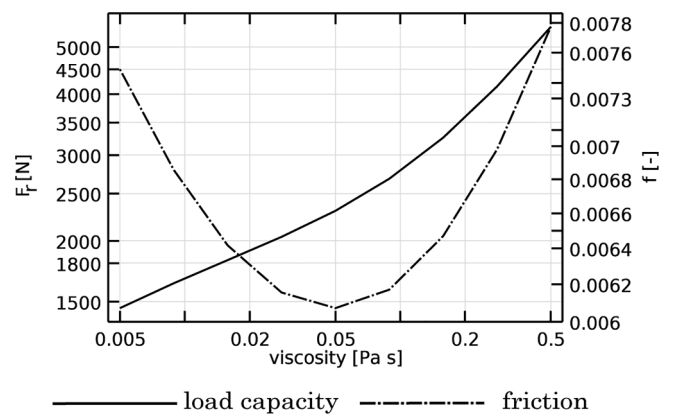


Fig. 12. Load and friction of the herringbone bearing as a function of the viscosity at the rheological textures. Note that the viscosity of the bulk is 0.05Pas.

rotational speed of 100 rpm. In this calculation, the yield stress is assumed to be zero everywhere in order to provide an easier comparison between the conventional bearing configuration and the bearing configuration with rheological texture. The results in Fig. 10 allow us to neglect the yield stress since it has only a minor effect on the load capacity and friction coefficient.

Fig. 12 shows an increase in load capacity for an increase in viscosity at the location of the rheological texture. This can be explained by the fact that the average viscosity of the lubricant within bearing gap increases. The friction force shows a minimum in friction at the point where the viscosity of the rheological texture is the same as the viscosity of the bulk. From this evidence, it seems that the use of the rheological texture in this bearing configuration always leads to an increase in friction coefficient.

Additional advantage of this concept is that the local viscous behaviour can be controlled, and thus the behaviour of the bearing can be modified during operation.

In general, the results presented in this work clearly demonstrate the power of the method to model the behaviour of a Bingham plastic in a lubricating film, as previously published by the authors in [31].

A possible and interesting next step in this research would be a shape optimization study of rheological textures that might increase the bearing performance. With the results herein presented, a fair comparison can be made between optimized rheological textures and optimized physical textures.

#### 4. Conclusion

The work has shown that bearing performance can be enhanced by using rheological textures. This principle adds an extra parameter in the design of a bearing that can be used to boost the performance. The potential of this concept is illustrated by comparing different bearing designs. Generally, the results show an increase in specific load capacity but also an increase in friction coefficient.

A new hybrid journal bearing configuration using the rheological texture is proposed where both hydrostatic and hydrodynamic working regimes are not compromised.

#### Declaration of Competing Interest

The authors declare that they have no known competing financial interests or personal relationships that could have appeared to influence the work reported in this paper.

#### Acknowledgment

This research has been supported by the Dutch TKI maritime funding program.

#### Appendix A. Supplementary data

Supplementary data to this article can be found online at <https://doi.org/10.1016/j.jmmm.2019.166218>.

#### References

- [1] S.S. Perry, W.T. Tysoe, Frontiers of fundamental tribological research, *Tribol. Lett.* 19 (2005) 151–161, <https://doi.org/10.1007/s11249-005-6142-8>.
- [2] N.K. Myshkin, I.G. Goryacheva, Tribology: trends in the half-century development, *J. Frict. Wear.* 37 (2016) 513–516, <https://doi.org/10.3103/S106836661606009X>.
- [3] P. Jost, Lubrication (Tribology) – A report on the present position and industry's needs, 1966.
- [4] K. Holmberg, A. Erdemir, Influence of tribology on global energy consumption, costs and emissions, *Friction* 5 (2017) 263–284, <https://doi.org/10.1007/s40544-017-0183-5>.
- [5] S. Glavatskih, E. Höglund, Tribotronics-towards active tribology, *Tribol. Int.* 41 (2008) 934–939, <https://doi.org/10.1016/j.triboint.2007.03.001>.
- [6] Y. Liu, S. Niu, Z.L. Wang, Theory of tribotronics, *Adv. Electron. Mater.* 1 (2015) 1500124–1500134, <https://doi.org/10.1002/aelm.201500124>.
- [7] S.G.E. Lampaert, J.W. Spronck, R.A.J. van Ostayen, Load and stiffness of a planar ferrofluid pocket bearing, *Proc. Inst. Mech. Eng. Part J J. Eng. Tribol.* 232 (2017) 14–25, <https://doi.org/10.1177/1350650117739200>.
- [8] S.G.E. Lampaert, B.J. Fellingner, J.W. Spronck, R.A.J. van Ostayen, In-plane friction behaviour of a ferrofluid bearing, *Precis. Eng.* 54 (2018) 163–170, <https://doi.org/10.1016/j.precisioneng.2018.05.013>.
- [9] M. Holmes, D. Trumper, Magnetic/fluid-bearing stage for atomic-scale motion control (the angstrom stage), *Precis. Eng.* 18 (1996) 38–49, [https://doi.org/10.1016/0141-6359\(95\)00038-0](https://doi.org/10.1016/0141-6359(95)00038-0).
- [10] W. Ochonski, Sliding bearings lubricated with magnetic fluids, *Ind. Lubr. Tribol.* 59 (2007) 252–265, <https://doi.org/10.1108/00368790710820856>.
- [11] H. Urreta, Z. Leicht, A. Sanchez, A. Agirre, P. Kuzhir, G. Magnac, Hydrodynamic bearing lubricated with magnetic fluids, *J. Intell. Mater. Syst. Struct.* 21 (2010) 1491–1499, <https://doi.org/10.1177/1045389X09356007>.
- [12] X. Wang, H. Li, G. Meng, Rotordynamic coefficients of a controllable magnetorheological fluid lubricated floating ring bearing, *Tribol. Int.* 114 (2017) 1–14, <https://doi.org/10.1016/j.triboint.2017.04.002>.
- [13] J. Hesselbach, C. Abel-Keilhack, Active hydrostatic bearing with magnetorheological fluid, *Proc. Eighth Int. Conf. New Actuators* (2002) 343–346, <https://doi.org/10.1063/1.1555850>.
- [14] J. Hesselbach, C. Abel-Keilhack, Active hydrostatic bearing with magnetorheological fluid, *J. Appl. Phys.* 93 (2003) 8441–8443, <https://doi.org/10.1063/1.1555850>.
- [15] J.M. Guldbakke, C. Abel-Keilhack, J. Hesselbach, Magnetofluidic Bearings and Dampers J.M., in: *Colloid. Magn. Fluids Basics, Dev. Appl. Ferrofluids*, 2009.
- [16] D. Brousseau, E.F. Borra, M. Rochette, D.B. Landry, Linearization of the response of a 91-actuator magnetic liquid deformable mirror, *Opt. Express* 18 (2010) 8239–8250, <https://doi.org/10.1364/OE.18.008239>.
- [17] D.A. Bompos, P.G. Nikolakopoulos, Rotordynamic analysis of a shaft using magnetorheological and nanomagnetorheological fluid journal bearings, *Tribol. Trans.* 59 (2016) 108–118, <https://doi.org/10.1080/10402004.2015.1050137>.
- [18] D.A. Bompos, Tribological Design of Nano/Magnetorheological Fluid Journal Bearings, 2015.
- [19] D.A. Bompos, P.G. Nikolakopoulos, CFD simulation of magnetorheological fluid journal bearings, *Simul. Model. Pract. Theory.* 19 (2011) 1035–1060, <https://doi.org/10.1016/j.simpat.2011.01.001>.
- [20] N. Vaz, K.G. Binu, P. Serrao, M.P. Hemanth, J. Jacob, N. Roy, E. Dias, Experimental investigation of frictional force in a hydrodynamic journal bearing lubricated with magnetorheological fluid, *J. Mech. Eng. Autom.* 7 (2017) 131–134, <https://doi.org/10.5923/j.jmea.20170705.01>.
- [21] A. Bouzidane, M. Thomas, An electrorheological hydrostatic journal bearing for controlling rotor vibration, *Comput. Struct.* 86 (2008) 463–472, <https://doi.org/10.1016/j.compstruc.2007.02.006>.
- [22] O.-O. Christidi-Loumpasefski, I. Tzifas, P.G. Nikolakopoulos, C.A. Papadopoulos, Dynamic analysis of rotor – bearing systems lubricated with electrorheological fluids, *Proc. Inst. Mech. Eng. Part K J. Multi-Body Dyn.* (2017) 1–16, <https://doi.org/10.1177/1464419317725932>.
- [23] J.S. Basavaraja, S.C. Sharma, S.C. Jain, A study of misaligned electrorheological fluid lubricated hole-entry hybrid journal bearing, *Tribol. Int.* 43 (2010) 1059–1064, <https://doi.org/10.1016/j.triboint.2009.12.052>.
- [24] S.C. Sharma, C.B. Khatri, Electro-rheological fluid lubricated textured multi-lobe hole-entry hybrid journal bearing system, *J. Intell. Mater. Syst. Struct.* 29 (2018) 1600–1619, <https://doi.org/10.1177/1045389X17742731>.
- [25] G.W. Stachowiak, A.W. Batchelor, *Engineering Tribology*, fourth ed., Elsevier Inc., 2014.
- [26] A. Singh, S.S. Waydande, A review paper on performance analysis of hydrodynamic journal bearing with various types of lubricant for pressure distribution and cavitation, *Int. J. Adv. Eng. Res. Dev.* 4 (2017) 347–354.
- [27] L. Lentini, M. Moradi, F. Colombo, A historical review of gas lubrication: from Reynolds to active compensations, *Tribol. Ind.* 40 (2018) 165–182, <https://doi.org/10.24874/ti.2018.40.02.01>.
- [28] S.G.E. Lampaert, R.A.J. van Ostayen, Load and stiffness of a hydrostatic bearing lubricated with a bingham plastic fluid, *J. Intell. Mater. Syst. Struct.* (2019).
- [29] S.G.E. Lampaert, R.A.J. Van Ostayen, Experimental results on a hydrostatic bearing lubricated with a magnetorheological fluid, *Curr. Appl. Phys.* (2019) in review.
- [30] S.G.E. Lampaert, R.A.J. van Ostayen, Lubricated Sliding Bearing With Adjustment Of The Properties Of The Lubricant In Certain Parts Of The Bearing Gap, WO2018212657, 2018.
- [31] S.G.E. Lampaert, R.A.J. van Ostayen, A lubrication theory for bingham plastics, *Tribol. Int.* (2020) in review.
- [32] C. Dorier, J. Tichy, Behavior of a Bingham-like viscous fluid in lubrication flows, *J. Nonnewton Fluid Mech.* 45 (1992) 291–310, [https://doi.org/10.1016/0377-0257\(92\)80065-6](https://doi.org/10.1016/0377-0257(92)80065-6).
- [33] S.H.K. Wada, Hayashi, Haga, Behavior of a Bingham solid in hydrodynamic lubrication (Part 1, General Theory) *Bull. Bull. JSME.* 16 (92) (1973) 422–431.
- [34] S. Wada, H. Hayashi, K. Haga, Behavior of a Bingham solid in hydrodynamic lubrication (Part 2, Application to Step Bearing), *Bull. JSME.* 16 (1973) 432–440, <https://doi.org/10.1299/jsme1958.16.422>.
- [35] S. Wada, H. Hayashi, K. Haga, Behavior of a bingham solid in hydrodynamic lubrication (part 3, application to journal bearing), *Bull. JSME* (1974) 1182.
- [36] J.A. Tichy, Hydrodynamic lubrication theory for the Bingham plastic flow model, *J. Rheol.* 35 (4) (1991) 477–496, <https://doi.org/10.1122/1.550231>.